Progress In Electromagnetics Research M, Vol. 110, 197–209, 2022

Quad Element Tree Shaped MIMO Antenna for Ultra-Wide Band Applications

Chiranjeevi Reddy Sereddy and Usha D. Yalavarthi*

Abstract—A compact and novel quad element MIMO antenna is presented for ultra-wideband (UWB) applications. The proposed orthogonal MIMO antenna comprises four identical elliptical structure-based tree shape microstrip line fed radiating elements. Radiating elements are placed in orthogonal with each other to obtain low mutual coupling and good diversity characteristics among MIMO elements. The proposed MIMO antenna operates from 4.2 GHz–13.2 GHz with an impedance bandwidth ($S_{11} < -10$ dB) of 9 GHz. It is investigated at 5.9 GHz DSRC band for vehicular communication applications and X-band for FSS applications. It exhibits superior characteristics with a peak gain of 6.2 dB at 11.7 GHz and radiation efficiency above 80%. To assess diversity performance of the proposed antenna MIMO performance metrics are investigated. Mean effective gain (MEG) < -3 dB, envelope correlation coefficient (ECC) < 0.05, channel capacity loss (CCL) < 0.4 bits/sec/Hz, diversity gain > 9.99, and multiplexing efficiency > -3 dB. Simulation results and experimentally obtained results are in fine agreement.

1. INTRODUCTION

Frequency range 3.1 GHz–10.6 GHz was allocated to ultra-wideband (UWB) commercial applications by Federal Communication Commission (FCC) [1]. However, it was mostly limited to indoor applications due to multipath fading and low data transmission and limited power spectral density of UWB. MIMO systems have the capability of enhancing spatial multiplexing gain thereby increasing spectral efficiency [2, 3]. These days, UWB is finding its own way in emerging automotive communications. Many researchers have proposed various UWB antennas, and demand for UWB MIMO antennas is still live. MIMO antenna system multiplexing efficiency analysis is discussed in [4]. UWB MIMO antennas for various applications like automotive, portable devices and with different methods and structures to enhance isolation are presented by various authors in [5–16]. Spatial and polarization diversity UWB MIMO antenna with circular polarization and improved performance is implemented in [17]. The authors in [18, 19] present a UWB MIMO antenna with low coupling using vias. Miniaturized and asymmetric CPW-fed UWB MIMO antennas are proposed in [20, 21]. In [22], a transparent ultra-wide band MIMO antenna is presented for automotive applications. A compact UWB antenna with CPW feeding technique and high isolation is presented in [23]. A wearable UWB MIMO antenna with reduced coupling is proposed and analyzed with SAR analysis in [24].

This paper presents an elliptical structured based tree shape orthogonal MIMO antenna for UWB applications, and its performance has been investigated for DSRC, X-band, and FSS frequency bands. Section 2 describes the design of proposed single element antenna, S_{11} characteristics, parametric analysis for performance optimization, gain, and radiation efficiency characteristics. Section 3 discusses two port and four port orthogonal MIMO antennas, S-parameter, and far-field radiation characteristics. Further fabricated quad element MIMO antenna, its measurement setup using VNA and an anechoic

Received 6 April 2022, Accepted 19 May 2022, Scheduled 6 June 2022
* Corresponding author: Usha Devi Yalavarthi (ushadevi.yalavarthi@kluniversity.in).
The authors are with the Department of ECE, Koneru Lakshmaiah Education Foundation, AP, India.

chamber are illustrated. Section 4 presents the discussion of measured and simulated results, and MIMO antenna performance metrics like ECC, TARC, DG, MEG, CCL, and multiplexing efficiency "η_{mux}" are examined. Section 5 gives the evaluation of proposed quad element MIMO antenna with relevant present works from literature. Section 6 concludes the work presented in this paper.

2. UWB ANTENNA

A UWB antenna with microstrip feedline method is proposed on an FR-4 substrate of size $26 \times 26 \times 0.8\,\text{mm}^3$. Radiating element is a tree-shaped patch that is designed using 5 consecutive elliptical structures E_1, E_2, E_3, E_4, and E_5 with major radii 6 mm, 7 mm, 8 mm, 9 mm, and 6 mm and ratio 0.25, respectively. Bottom layer consists of a defected ground structure (DGS) with ground length L_g. Simulated proposed antenna single element configuration and geometrical specifications are presented in Figure 1 and Table 1, respectively.

Table 1. Geometrical specifications of proposed tree shape antenna.

Parameter	L_s	W_s	L_f	W_f	L_g
Dimensions (mm)	26	26	10.5	2	9.5

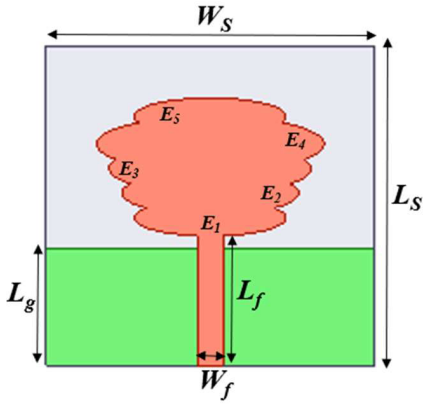

Figure 1. Geometrical configuration of proposed tree shape antenna.

Figure 2 describes S_{11} and VSWR features of the proposed tree shape antenna. It operates from 4.56–13.29 GHz with a bandwidth of 8.73 GHz for $S_{11} < -10$ dB. Parametric analysis for changes in feed-width (W_f) and ground plane length (L_g) is performed as resonant frequency shifts with variations in ground plane and feed-width. S_{11} characteristics obtained from parametric analysis are presented in Figures 3(a) and 3(b). For $L_g = 9.5$ mm and $W_f = 2$ mm, the proposed antenna operates for wide-band. Gain and radiation efficiency curves of the projected tree shape antenna are represented in Figure 4. Peak gain ranges from 2.3 dB to 5.5 dB, and radiation efficiency is not less than 85%.

3. ORTHOGONAL MIMO ANTENNA

3.1. Two Port MIMO Antenna

A two port orthogonal MIMO antenna is developed from the proposed single element as represented in Figure 5(a). MIMO antenna elements M_1 and M_2 are placed orthogonally and in opposite planes to achieve good diversity characteristics and isolation. The proposed MIMO antenna top layer consists of an M_1 radiating patch and M_2 ground plane, where bottom layer consists of M_1 ground plane and M_2

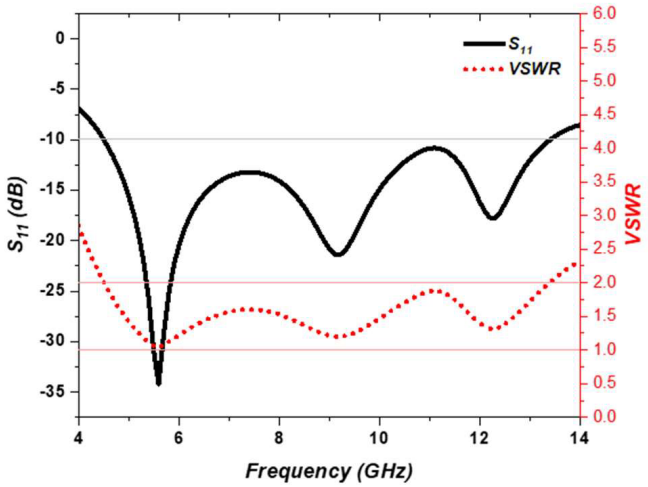

Figure 2. S_{11} and VSWR curves of proposed antenna.

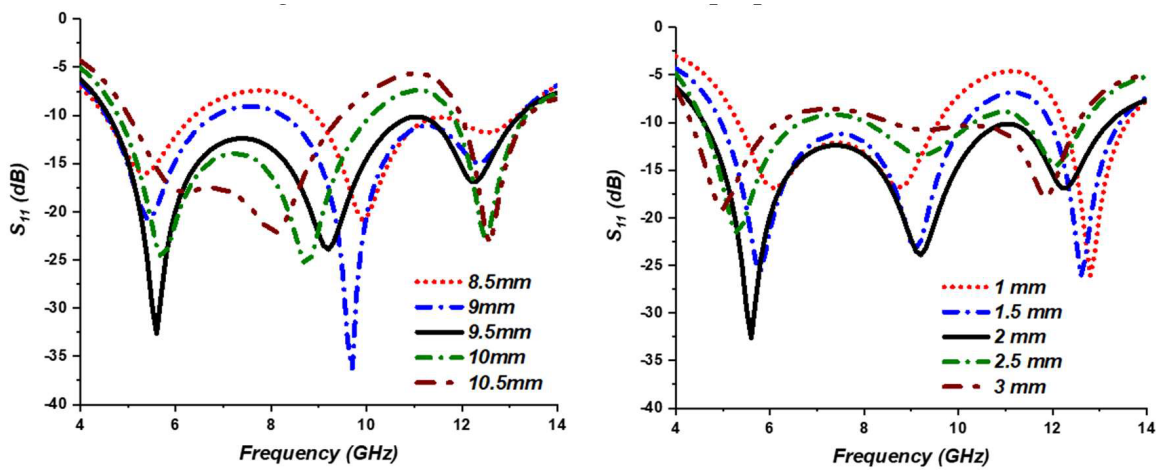

(a) Changes in *Lg* (b) Changes in *Wf*

Figure 3. Parametric analysis of proposed tree shape antenna.

radiating patch. Surface current distribution for port-1 excitation is illustrated in Figure 5(b). With a simple structure, mutual coupling between two ports is very low as shown in Figure 5(b).

S-parameter features of the two port orthogonal MIMO antenna are illustrated in Figure 6. S_{11} and S_{22} curves deviate slightly but still obtain same ultra-wide operating band from 4.2–13.2 GHz. S_{12} and S_{21} curves overlap as two MIMO elements M_1 and M_2 are identical, and isolation is greater than 25 dB. Figure 7 presents gain characteristics of two MIMO elements M_1 and M_2. M_1 element exhibits a peak gain of 5.2 dB at 5.9 GHz whereas M_2 element exhibits a peak gain of 6 dB at 10 GHz.

Radiation efficiency of the proposed two port MIMO antenna ranges from 93% to 82% in the entire operating band with slight variations in M_1 and M_2 curves as presented in Figure 8. Though M_1 and M_2 elements are identical, minor deviations are observed in S_{11} and S_{22} values and gain and radiation efficiency characteristics due to non-symmetry of their arrangement on substrate.

3.2. Four Port MIMO Antenna

Figure 9(a) illustrates a quad port MIMO antenna with four MIMO elements M_1, M_2, M_3, and M_4 placed orthogonally and in opposite layers. M_1 and M_3 are placed on the top layer, and respective

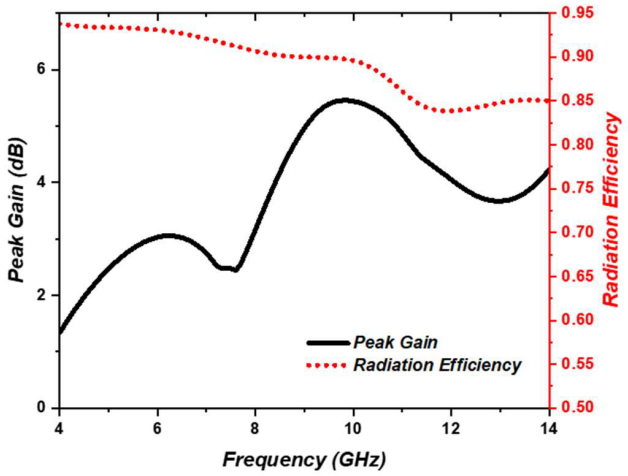

Figure 4. Gain and radiation efficiency curves of proposed tree shape antenna.

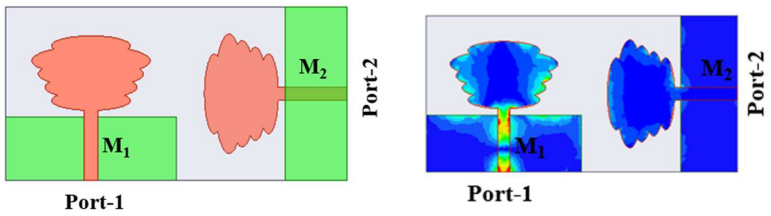

(a) Geometrical configuration (b) Surface current distribution

Figure 5. Two port orthogonal MIMO antenna.

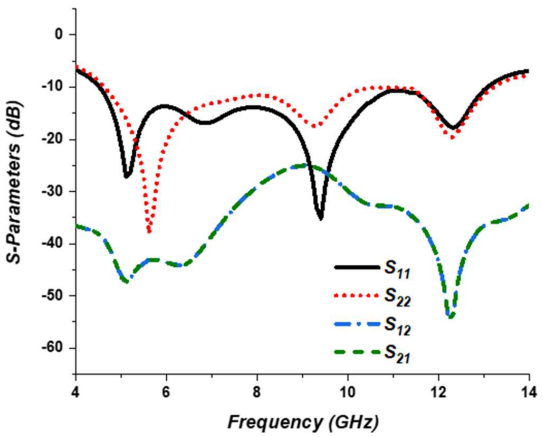

Figure 6. S-parameter curves of two port orthogonal MIMO antenna.

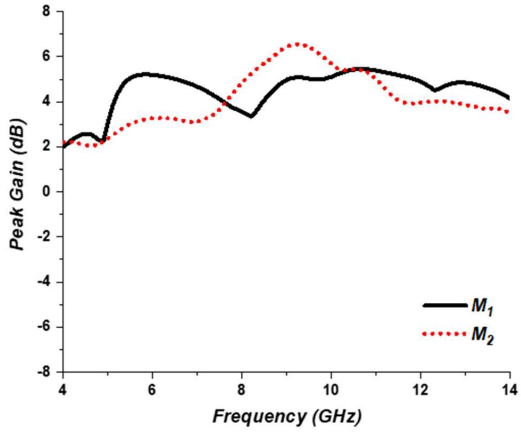

Figure 7. Gain characteristics of two port orthogonal MIMO antenna.

ground planes lie on the bottom layer. M_2 and M_4 are placed on the bottom layer, and respective ground planes lie on the top layer. Figures 9(b) and 9(c) present the top view and bottom view of fabricated antenna model. Investigational arrangement of the proposed MIMO antenna on VNA is presented in Figure 10.

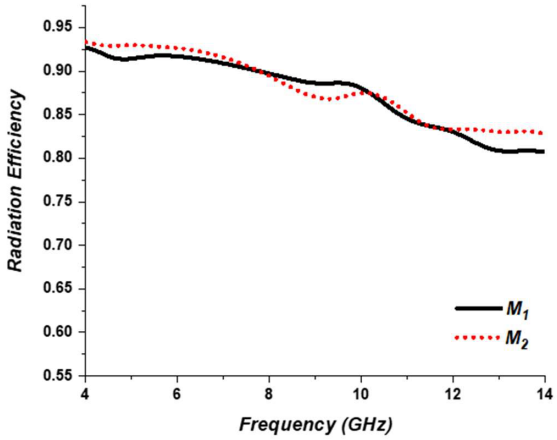

Figure 8. Radiation efficiency characteristics of two port orthogonal MIMO antenna.

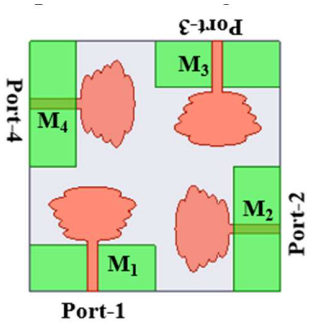

(a) Simulated quad element MIMO antenna

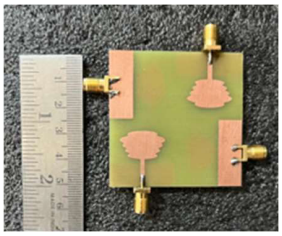

(b) Antenna top view

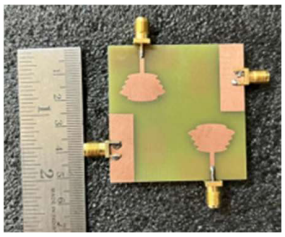

(c) Antenna bottom view

Figure 9. Proposed quad port orthogonal MIMO antenna.

4. RESULTS AND DISCUSSIONS

4.1. *S*-Parameters

Measured and simulated S-parameter curves of the quad port MIMO antenna for port-1 excitation are presented in Figure 11. S-parameter characteristics are measured experimentally on VNA by exciting one port and terminating other ports using 50 ohm load impedance. Figure 11(a) illustrates simulated and measured reflection coefficient (S_{11}) characteristics of the proposed antenna. Measured S_{11} characteristics on VNA are also presented for validating the results (Figure 10). The fabricated proposed antenna operates from 5.45 GHz to 13.05 GHz for $S_{11} < -10$ dB. It achieves an impedance bandwidth of 7.6 GHz suitable for DSRC, X-band, and FSS applications. Figure 11(b) represents simulated and measured transmission coefficient (S_{21}, S_{31} and S_{41}) characteristics of the proposed antenna. Measured transmission coefficients show that the coupling among MIMO antenna elements is less than 25 dB, and measured characteristics are close to simulation ones with minor deviations.

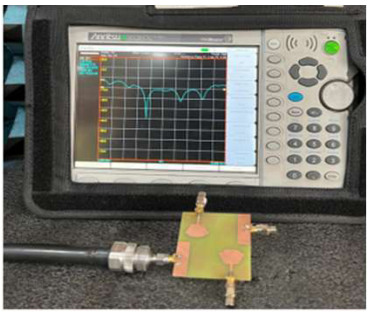

Figure 10. Experimental setup of proposed MIMO antenna.

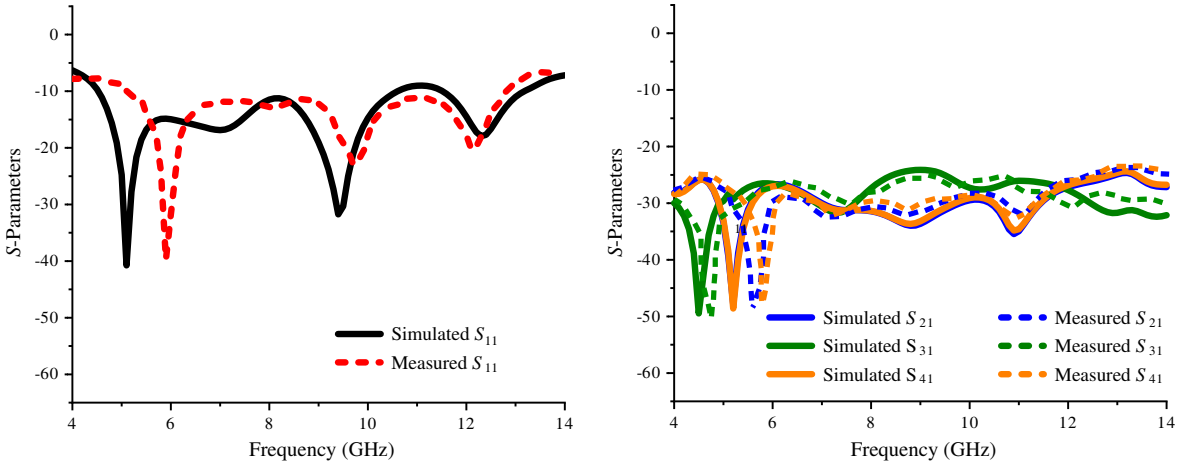

(a) Reflection coefficient characteristics (b) Transmission coefficient characteristics

Figure 11. *S*-parameter features of proposed quad port orthogonal MIMO antenna.

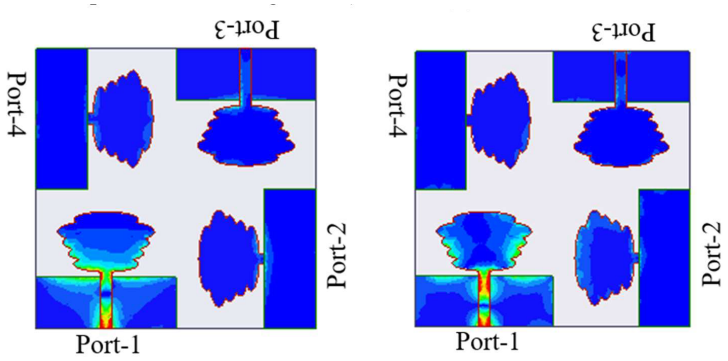

(a) 5.9 GHz (b) 10.5 GHz

Figure 12. Current distribution of proposed quad element MIMO antenna.

4.2. Current Distribution and Far-Field Radiation Characteristics

Figure 12 represents current distribution of the proposed quad port MIMO antenna for M_1 excitation at 5.9 GHz and 10.5 GHz. When port-1 is excited, ports-2, 3, 4 are very weakly coupled, and it is visible through current distribution presentation in Figures 12(a) and 12(b).

Gain plot of the proposed antenna (M_2 element) at 5.9 GHz is illustrated in Figure 13(a).

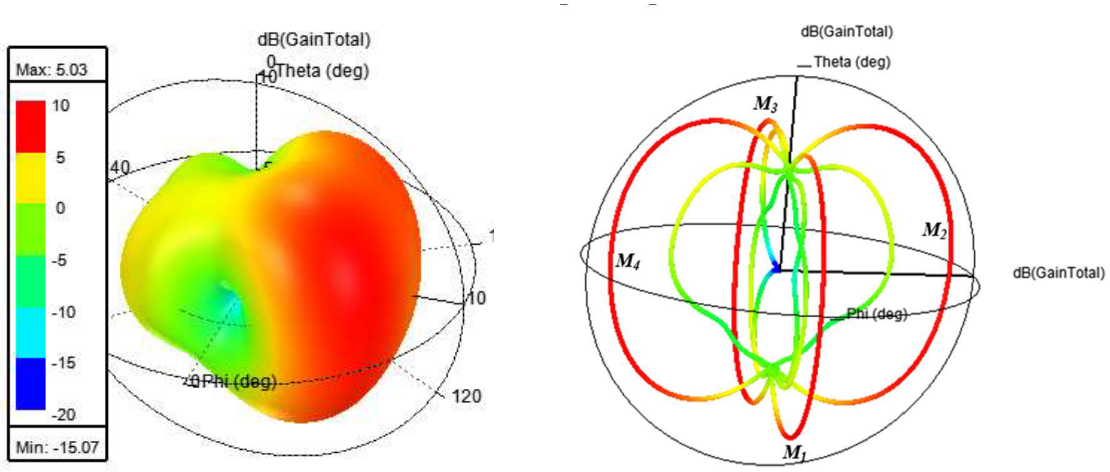

(a) 3D gain plot of M_2 element (b) Gain plots of all elements

Figure 13. Gain plot of proposed MIMO antenna at 5.9 GHz.

Orthogonality of the proposed MIMO antenna is validated from Figure 13(b) which presents the gain plot of all MIMO elements (M_1, M_2, M_3, and M_4) for Phi = 0 (Ports-1 and 3) and Phi = 90° (ports-2 and 4). Gain patterns of MIMO elements are orthogonal with respective to consecutive elements.

Figure 14(a) presents the simulated radiation pattern of all MIMO elements at 5.9 GHz in phi plane for theta = 90°, and it validates the orthogonality of MIMO antenna. Figures 14(b), (c), and (d) represent the radiation patterns of M_1 and M_3 elements at 5.9 GHz and 10 GHz.

Gain characteristics of port-1 (M_1 element) are presented in Figure 15. Gain varies from 4.2 dB to 6.2 dB in the entire operating band, and peak gain of 6.2 dB is attained at 11.7 GHz. Gain characteristics of other ports (M_2, M_3, and M_4) are almost similar due to identical structures of MIMO elements. Radiation efficiency of the proposed MIMO antenna ranges between 91.3 and 80% as illustrated in Figure 16.

4.3. MIMO Performance Metrics

4.3.1. Envelope Correlation Coefficient

ECC between MIMO elements is obtained from S-parameters or radiation patterns. If radiation efficiency of an antenna is less than 97%, ECC values obtained from S-parameters may yield error greater than 10%. Therefore, radiation patterns are used to obtain ECC values as shown in Equation (1).

$$ECC = \frac{\left|\int_0^{2\pi}\int_0^{\pi}\left(XPR\,E_{\theta 1}E_{\theta 2}^{*}P_{\theta}+E_{\varphi 1}E_{\varphi 2}^{*}P_{\varphi}\right)d\Omega\right|^2}{\int_0^{2\pi}\int_0^{\pi}\left(XPR\,E_{\theta 1}E_{\theta 1}^{*}P_{\theta}+E_{\varphi 1}E_{\varphi 1}^{*}P_{\varphi}\right)d\Omega X\int_0^{2\pi}\int_0^{\pi}\left(XPR\,E_{\theta 2}E_{\theta 2}^{*}P_{\theta}+E_{\varphi 2}E_{\varphi 2}^{*}P_{\varphi}\right)d\Omega} \quad (1)$$

$ECC(n,m)$ represents the correlation coefficient between ports n and m where $m \neq n$. As all MIMO elements are alike, $ECC(n,m) = ECC(m,n)$. For $ECC < 0.5$, MIMO antenna shows better diversity performance and uncorrelated radiation patterns. The proposed MIMO antenna obtains $ECC < 0.045$ in the entire operating band as presented in Figure 17. At resonant frequencies 5.9 GHz and 10 GHz, ECC values are less than 0.01.

4.3.2. Diversity Gain

The diversity gain of MIMO antenna is obtained from ECC values using Equation (2).

$$DG = 10\sqrt{1 - ECC^2} \quad (2)$$

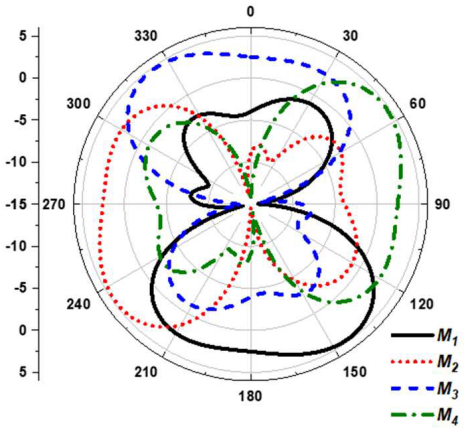

(a) 5.9 GHz for Theta = 90° in Phi plane

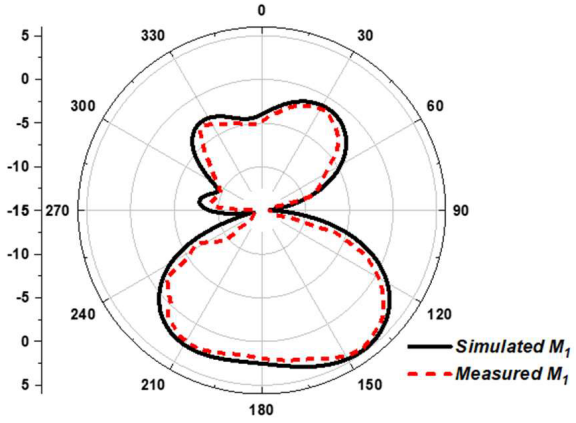

(b) 5.9 GHz for Theta = 90° in Phi plane

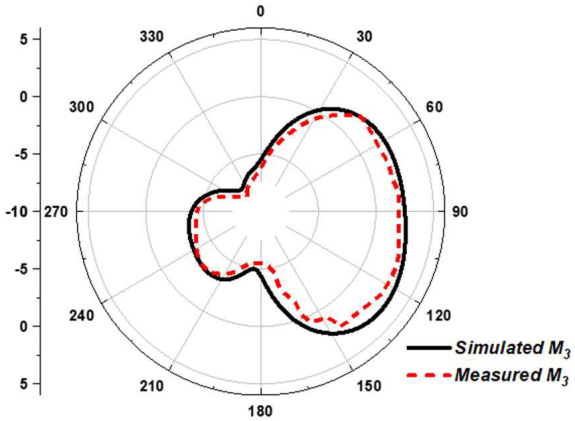

(c) 5.9 GHz for Phi = 0° in Theta plane

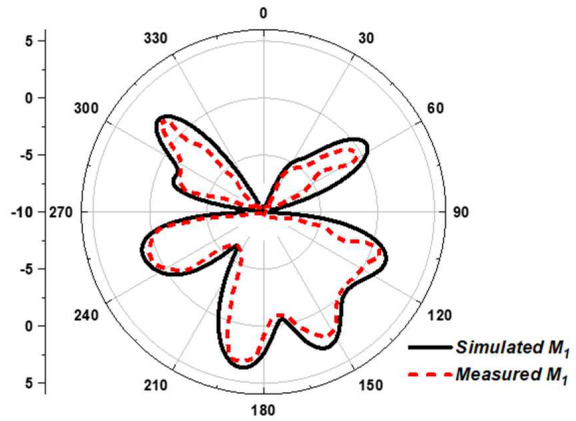

(d) 10 GHz for Theta = 90° in Phi plane

Figure 14. Radiation patterns of proposed quad port MIMO antenna.

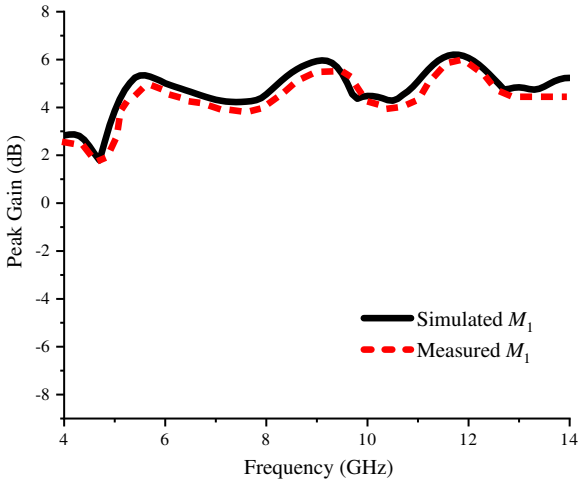

Figure 15. Gain characteristics of proposed quad port MIMO antenna.

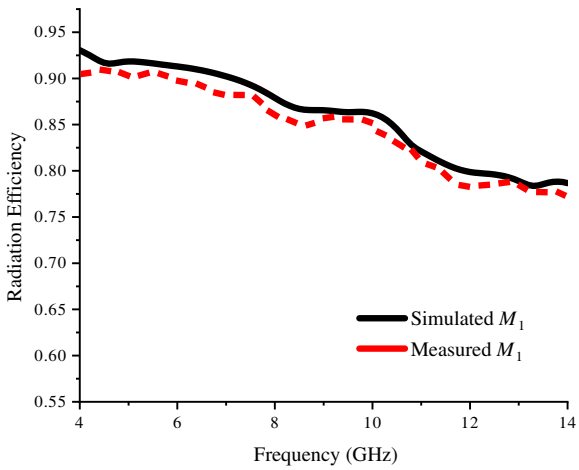

Figure 16. Radiation efficiency curves of proposed quad port MIMO antenna.

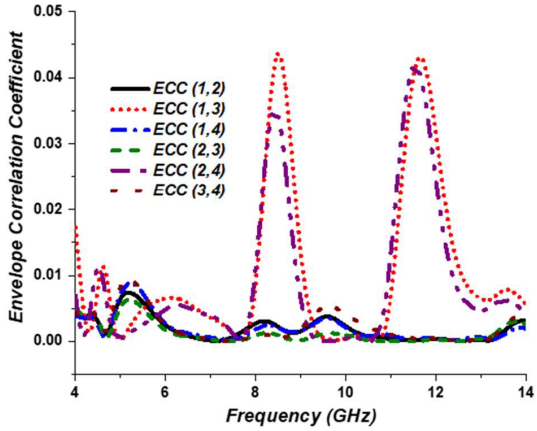

Figure 17. ECC characteristics of proposed MIMO antenna.

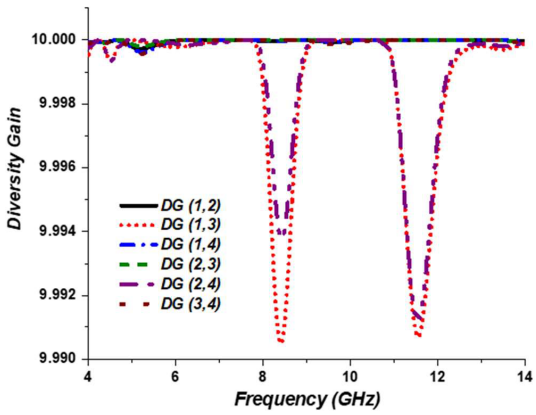

Figure 18. Diversity gain characteristics of proposed MIMO antenna.

$DG(n, m)$ represents the diversity gain between ports n and m where $DG(n, m) = DG(m, n)$ and $n \neq m$. Figure 18 illustrates DG characteristics of the proposed MIMO antenna, and DG values are greater than 9.99 (close to 10). Therefore, the projected MIMO antenna exhibits better diversity performance.

4.3.3. Mean Effective Gain

The MEG of MIMO antenna with "n" ports is obtained from S-parameters as shown in Equation (3), where i is the port or MIMO element number. To have good diversity among MIMO elements, MEG_i should range between $-12\,\text{dB} < MEG_i < -3\,\text{dB}$ and ratios MEG_1/MEG_2, MEG_1/MEG_3, etc. which should be less than 3 dB.

$$MEG_i = 0.5\left[1 - \sum_{j=1}^{n} |S_{ij}|^2\right] \tag{3}$$

Figure 19(a) presents MEG_1 of the proposed quad port MIMO antenna for port-1, and other ports' MEG is same as MEG_1 with minute variations as all MIMO elements are identical. MEG_1 is less than $-3\,\text{dB}$ and greater than $-12\,\text{dB}$ as presented in Figure 19(a). Figure 19(b) represents ratios of MEG

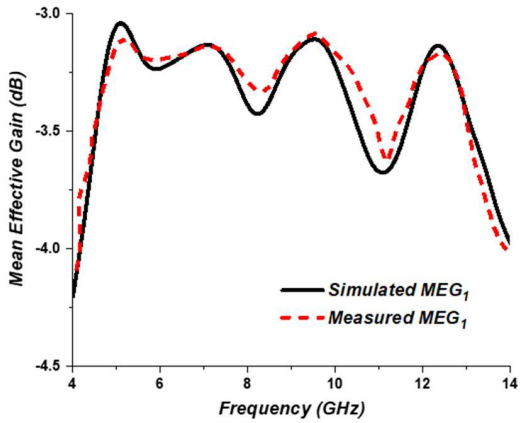

(a) MEG of M_1

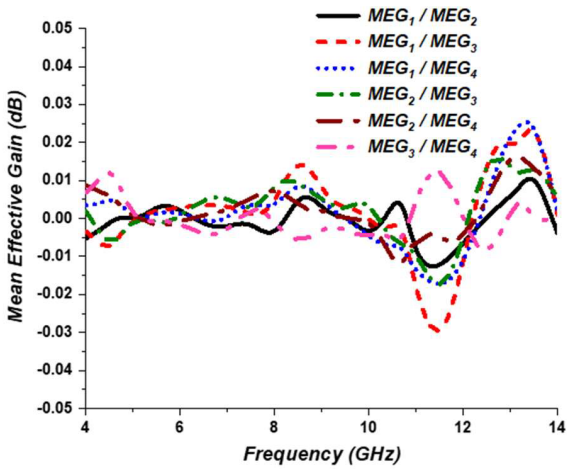

(b) Ratio of MEG at all ports

Figure 19. MEG of proposed quad port MIMO antenna.

at ports 1, 2, 3, and 4. As shown in Figure 19(b), ratios of MEG are very close to 0 dB which indicate that the MEGs of all MIMO elements are almost the same.

4.3.4. Total Active Reflection Coefficient

TARC defines MIMO antenna effective operating bandwidth with multiple ports. It is achieved from S-parameters (two port network) as given in Equation (4).

$$\Gamma_a^t = \sqrt{\frac{\left(\left(|S_{11} + S_{12}e^{j\theta}|^2\right) + \left(|S_{21} + S_{22}e^{j\theta}|^2\right)\right)}{2}} \tag{4}$$

where θ is the input feeding phase.

Figure 20 illustrates TARC characteristics of the proposed quad element MIMO antenna for $\theta = 0°$. Effective operating band ($S_{11} < -10$ dB) achieved is from 4.55 GHz to 13.15 GHz with minute deviations at 8 GHz and 11 GHz.

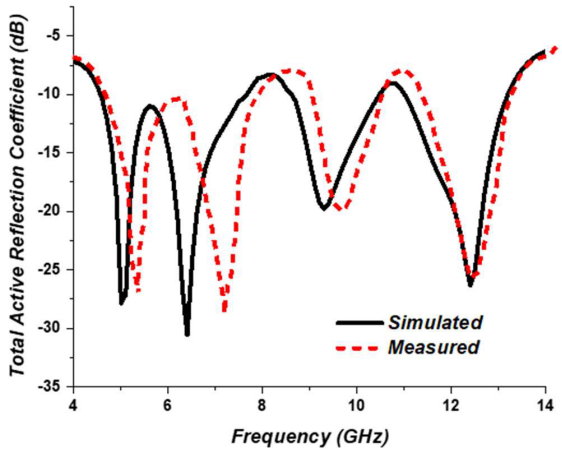

Figure 20. TARC of proposed MIMO antenna.

4.3.5. Channel Capacity Loss

In communication channel, CCL gives the maximum limit for lossless transmission. Usually, $CCL < 0.4$ bits/sec/Hz to support lossless transmission in MIMO system. CCL is obtained using S-parameter values as presented in Equations (5)–(8). The proposed MIMO antenna achieves CCL values not greater than 0.4 bits/sec/Hz in operating band as presented in Figure 21 (black dotted curve).

$$CCL = -\log_2\left(\det\left(\psi^R\right)\right) \tag{5}$$

where,

$$\psi^R = \begin{vmatrix} \rho_{11} & \rho_{12} & \rho_{13} & \rho_{14} \\ \rho_{21} & \rho_{22} & \rho_{23} & \rho_{24} \\ \rho_{31} & \rho_{32} & \rho_{33} & \rho_{34} \\ \rho_{41} & \rho_{42} & \rho_{43} & \rho_{44} \end{vmatrix} \tag{6}$$

$$\rho_{ii} = 1 - \sum_{n=1}^{4} |S_{in}|^2 \tag{7}$$

$$\rho_{ij} = -\left(S_{ii}^* S_{ij} + S_{ji}^* S_{ij}\right) \tag{8}$$

4.3.6. Multiplexing Efficiency

η_{mux} determines MIMO antenna performance better evaluation in modest way. For quad port MIMO antenna, multiplexing efficiency (η_{mux}) can be calculated using Equations (9)–(15).

$$\eta_{\text{mux}} = \left[\left(\prod_{i=1}^{k} \eta_i\right) \cdot \det\left(\psi^P\right)\right]^{1/k} \tag{9}$$

where ψ^P is normalized antenna correlation matrix, and η_i is the total efficiency of ith antenna.

It is expressed using Equation (10):

$$\eta_{total} = \eta_{radiation} * \eta_{mismatch} + coupling \tag{10}$$

Figure 21 illustrates multiplexing efficiency of the proposed MIMO antenna. η_{mux} achieved is greater than -3 dB as shown in Figure 21 (red solid curve).

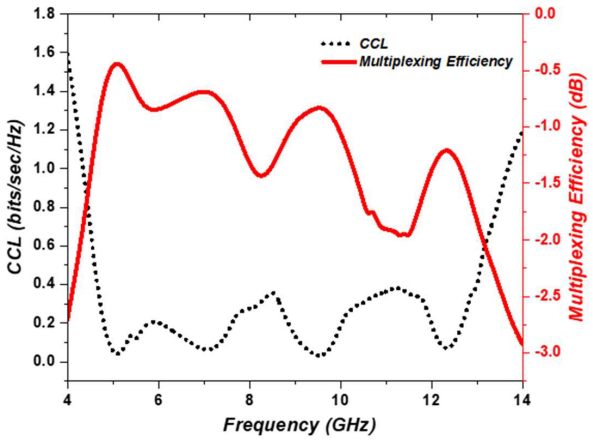

Figure 21. Multiplexing efficiency and CCL of proposed quad port MIMO antenna.

Table 2. Proposed MIMO antenna parameters comparison with relevant works.

Reference	T. Addepalli [16]	Qingzhi Yang [19]	A. A. Khan [20]	D. Potti [22]	Wenfei Yin [23]	Proposed
Dimensions (mm^3)	16×26	$34 \times 34 \times 1.6$	$40 \times 40 \times 1.524$	29×50	$38 \times 38 \times 1.6$	$52 \times 52 \times 0.8$
Bandwidth (GHz)	2.82–14.45	2.5–11.6	3–13.5	2.4–11	3–20	4.2–13.2
Ports	2	4	4	2	4	4
Gain (dB)	0.7–6.86	2–6	3.5	2	1.4–6.3	3–6.11
ECC	< 0.08	< 0.05	< 0.4	< 0.04	< 0.08	< 0.05
Isolation (dB)	> 22	> 18	> 15	> 20	> 17	> 25
MEG (dB)	-	-	-	-	-	< -3
CCL (bits/sec/Hz)	-	-	< 0.4	-	-	< 0.4
η_{mux} (dB)	-	-	> -3.5	-	> -3	> -3

5. COMPARISON

The comparison of MIMO antenna parameters like operating bandwidth, number of ports, gain, ECC, isolation, MEG, CCL, η_{mux}, and substrate material with other relevant models is tabulated in Table 2 from state-of-the-art literature. The proposed tree shape quad port MIMO antenna exhibits better isolation, gain, and diversity performance characteristics.

6. CONCLUSION

A quad port orthogonal MIMO antenna with elliptical structure-based tree shape is proposed for DSRC, X band, and FSS applications. Four MIMO elements are positioned in orthogonal to each other, and two MIMO elements M_2 and M_4 are placed in opposite layers with respect to MIMO elements M_1 and M_3. This achieved orthogonality property and better isolation between MIMO elements without using much complicated structures. S-parameters characteristics, far-field radiation characteristics (gain, radiation patterns, radiation efficiency), surface current distribution and MIMO metrics are examined to evaluate the proposed MIMO antenna performance. Gain of the proposed antenna ranges from 4.2 dB to 6.2 dB, and radiation efficiency is greater than 80%. ECC values obtained are less than 0.05; DG values are very near 10; MEG values are less than -3 dB and greater than -12 dB; CCL values are less than 0.4 bits/sec/Hz; multiplexing efficiency is greater than -3 dB; and effective operating band obtained from TARC characteristics closely resembles the operating band obtained from S-parameter characteristics. Simulated and practically obtained characteristics are in fine agreement. Therefore, the proposed orthogonal MIMO antenna is appropriate for DSRC, X-band, and FSS applications with better diversity performance characteristics and uncorrelated radiation patterns.

REFERENCES

1. FCC. Washington, DC, "FCC 1st report and order on ultra-wideband technology," FCC, Feb. 2002.
2. Kaiser, T., F. Zheng, and E. Dimitrov, "An overview of ultra-wide-band systems with MIMO," *Proceedings IEEE*, Vol. 97, 285–312, 2009.
3. Jiang, C. and L. J. Cimini, "Antenna selection for energy-efficient MIMO transmission," *IEEE Wireless Communication Letters*, Vol. 1, 577–80, 2012.
4. Tian, R., B. K. Lau, and Z. Ying, "Multiplexing efficiency of MIMO antennas," *IEEE Antennas Wireless Propagation Letters*," Vol. 10, 183–186, 2011.
5. Liu, L., S. W. Cheung, and T. I. Yuk, "Compact MIMO antenna for portable devices in UWB applications," *IEEE Transactions on Antennas and Propagation*, Vol. 61, 4257–4264, 2013.
6. Alsath, M. and M. Kanagasabai, "Compact UWB monopole antenna for automotive communications," *IEEE Transactions on Antennas and Propagation*, Vol. 63, 4204–4208, 2015.
7. Srivastava, G. and A. Mohan, "Compact MIMO slot antenna for UWB applications," *IEEE Antennas Wireless Propagation Letters*, Vol. 15, 1057–1060, 2016.
8. Deng, J. Y., L. X. Guo, and X. L. Liu, "An ultrawideband MIMO antenna with a high isolation," *IEEE Antennas Wireless Propagation Letters*, Vol. 15, 182–185, 2016.
9. Tao, J. and Q. Feng, "Compact ultrawideband MIMO antenna with half-slot structure," *IEEE Antennas and Wireless Propagation Letters*, Vol. 16, 792–795, 2017.
10. Sipal, D., M. P. Abegaonkar, and S. K. Koul, "Easily extendable compact planar UWB MIMO antenna array," *IEEE Antennas Wireless Propagation Letters*, Vol. 16, 2328–2331, 2017.
11. Li, H., J. Liu, Z. Wang, and Y.-Z. Yin, "Compact 1×2 and 2×2 MIMO antennas with enhanced isolation for ultrawideband application," *Progress In Electromagnetics Research C*, Vol. 71, 41–49, 2017.
12. Zhao, X., S. P. Yeo, and L. C. Ong, "Planar UWB MIMO antenna with pattern diversity and isolation improvement for mobile platform based on the theory of characteristic modes," *IEEE Transactions on Antennas and Propagation*, Vol. 66, 420–425, 2018.

13. Chandel, R., A. K. Gautam, and K. Rambabu, "Design and packaging of an eye-shaped multiple-input–multiple-output antenna with high isolation for wireless UWB applications," *IEEE Transactions on Components, Packaging and Manufacturing Technology*, Vol. 8, 635–642, 2018.
14. Nie, Y., X. Q. Lin, Z. Q. Yang, J. Zhang, and B. Wang, "Structure shared planar UWB MIMO antenna with high isolation for mobile platform," *IEEE Transactions on Antennas and Propagation*, Vol. 67, 2735–2738, 2019.
15. Wang, L., et al., "Compact UWB MIMO antenna with high isolation using fence-type decoupling structure," *IEEE Antennas and Wireless Propagation Letters*, Vol. 18, 1641–1645, 2019.
16. Addepalli, T. and V. R. Anitha, "A very compact and closely spaced circular shaped UWB MIMO antenna with improved isolation," *AEU — International Journal of Electronics and Communications*, Vol. 114, No. 9, 153016, 2020.
17. Ullah, U., I. B. Mabrouk, S. Koziel, and M. Al-Hasan, "Implementation of spatial/polarization diversity for improved-performance circularly polarized multiple-input-multiple-output ultra-wideband antenna," *IEEE Access*, Vol. 8, 64112–64119, 2020.
18. Singh, H. V. and S. Tripathi, "Compact UWB MIMO antenna with Fork-shaped stub with vias based coupling current steering (VBCCS) to enhance isolation using CMA," *AEU — International Journal of Electronics and Communications*, Vol. 129, No. 12, 153550, 2021.
19. Yang, Q., K. Wang, and Y. Sun, "Quad-port miniaturized ultra-wideband mimo antenna with metal vias," *Progress In Electromagnetics Research Letters*, Vol. 97, 95–103, 2021.
20. Khan, A. A., S. A. Naqvi, M. S. Khan, and B. Ijaz, "Quad port miniaturized MIMO antenna for UWB 11 GHz and 13 GHz frequency bands," *AEU — International Journal of Electronics and Communications*, Vol. 131, 153618, 2021.
21. Bharghava, P. and P. Muthusamy, "Compact asymmetric coplanar strip fed MIMO antenna with band dispension characteristics for UWB applications," *Progress In Electromagnetics Research C*, Vol. 115, 17–26, 2021.
22. Potti ,D., et al., "A novel optically transparent UWB antenna for automotive MIMO communications," *IEEE Transactions on Antennas and Propagation*, Vol. 69, 3821–3828, 2021.
23. Yin, W., S. Chen, J. Chang, C. Li, and S. K. Khamas, "CPW fed compact UWB 4-element MIMO antenna with high isolation," *Sensors*, Vol. 21, No. 8, 2688, 2021.
24. Rekha, S. and G. S. Let, "Design and SAR analysis of wearable UWB MIMO antenna with enhanced isolation using a parasitic structure," *Iran J. Sci. Technol. Trans. Electr. Eng.*, Vol. 46, 291–301, 2022.